Ageing of PEEK/Carbon Fibre composite under electronic irradiations: Influence on mechanical behaviour and charge transport

Guilhem Rival, Éric Dantras, Thierry Paulmier

Ageing of PEEK / Carbon Fibre composite under electronic irradiations: influence on mechanical behaviour and charge transport

Guilhem Rival[a,b,1], Éric Dantras[a,*], Thierry Paulmier[b],

[a] *CIRIMAT - Université Toulouse III Paul Sabatier, Physique des Polymères, 118 route de Narbonne, 31062 Toulouse, France*

[b] *ONERA - DPHY, The French Aerospace Lab, F-31055 Toulouse – France*

Abstract

Polymer used in satellite manufacturing are exposed to surface charging phenomenon due to electronic irradiations. This phenomenon can induce electrostatic discharges (ESD) which can lead to failures. In order to limit this phenomenon, we propose to develop PEEK composite reinforced with Short Carbon Fibres (SCF). We studied the behaviour of these composites in pristine state and after electronic irradiations compared to PEEK. In pristine state, fibres induce a faster surface electron relaxation. This behaviour shows that SCF can reduce ESD risks in space which is a first validation of the concept. After irradiations, PEEK ageing mechanisms are not modified by the presence of fibres. However, SCF stabilise both the evolution of mechanical behaviour and surface potential relaxation compared to irradiated PEEK. This stabilisation comes from two contributions: fibres stabilise the ageing of the matrix and hides the influence of this ageing on composite mechanical and electrical behaviours.

Keywords: A. Polymer-matrix composites (PMCs), Ionising Radiation, B. Electrical Properties, B. Mechanical Properties

1. Introduction

In geostationary earth orbit (GEO), materials used for spacecraft manufacturing are exposed to several environmental constraints like thermal cycling, micrometeorites and space debris impacts or irradiation by charged particles (*e.g.* protons, electrons). Especially for polymer materials, irradiation by electrons presents two main problematics for satellites.

* Corresponding author
Email address: eric.dantras@univ-tlse3.fr (Éric Dantras)
[1] Present address: Laboratoire de Génie Electrique et Ferroélectricité (LGEF), INSA Lyon, 69621 Villeurbanne, France

The first problematic concerns the ageing of polymers. It results from the energy transferred by electrons passing through material volume. This energy transfer induces an ionisation of the polymer which leads to modifications of its physico-chemical structure. Therefore, the polymer may no longer fulfill its main function and lead to satellite failures. Thus, it is essential to study polymer behaviour under electronic irradiations in order to better anticipate satellite lifetime in space environment. Recently, space industry started to use PolyEtherEtherKetone (PEEK), a high performance thermoplastic polymer, for structural applications in satellite manufacturing. This new polymer in space industry is intended to replace widely used thermoset matrices. Currently, PEEK is used in Carbon Fibre Reinforced Polymer as primary structure material for the articulated arm of the International Space Station [1] or as mechanical support for scientific instruments like the Search-Coil Magnetometer that embarked on the Parker Solar Probe mission [2]. The use of this polymer results, among other properties, from its high tolerance to ionising radiations (electronic or γ irradiations). Indeed, many works studied the ageing of PEEK under ionising radiations and highlighted evolutions of its structure and properties. Nonetheless, these evolutions are observed for very high deposited energies compared to other polymers. Hegazy *et al.* studied gas emissions during γ and electronic irradiations [3, 4]. They observed a release of CO and CO_2 for both irradiations and concluded that chain scissions occur mainly on ether and ketone functions. Moreover, they studied by Differential Scanning Calorimetry the influence of γ irradiations on PEEK thermal transitions [5]. They pointed out increase in glass transition temperature explained by a cross-linking phenomenon and a decrease in both melting temperature and crystallinity ratio due to the formation of defects in crystalline structures. The influence of this ageing on the PEEK properties has also been studied. Under electronic irradiations, Sasuga *et al.* reported evolutions of PEEK mechanical properties [6, 7]. For example, they observed a global degradation of its tensile properties like its elongation at break which decreases from 296 % for pristine sample to 52 % at 50 MGy due to cross-linking. On its electrical behaviour, Shinyama *et al.* use Broadband Dielectric Spectroscopy to bring into evidence a wider relaxation time distribution explained by the increase in amorphous phase heterogeneity due to cross-linking nodes [8, 9]. However, these studies were carried out in the framework of nuclear applications and therefore, irradiations were performed under air which is not representative of space environment.

The second problematic concerns charging phenomena induced by low energy electrons. Due to the dielectric nature of polymers, these electrons accumulate at the polymer surface. This accumulation leads to an increase of electrical surface potential (voltage levels of several kilovolts can be reached) and induces

electrostatic discharge (ESD) phenomena likely to degrade electronic systems. These ESDs are responsible for many spacecraft failures and anomalies in orbit [10]. Moreover, these charging phenomena are highly impacted by polymer ageing which can induces evolutions of its electrical properties and amplify electron accumulation. Optimisation of electrical properties of polymers is an important research axis for several application fields like anti-static materials [11], flexible electronics [12, 13] or aerospace industry [14, 15]. One of the ways to optimise charge transport is to develop polymer composites loaded with electrically conductive fillers (*e.g.* metallic particles). Indeed, above a certain particle ratio named percolation threshold p_c, the electrical conductivity brutally increases (about 10-15 decades) due to the formation of a conductive path between fillers [16]. This percolation threshold is dependent of filler aspect ratio and the conductivity above p_c is dependent of filler nature (carbon or metallic fillers). This concept could be a good solution for limiting charging phenomena on polymers. However, most of the polymer applications on satellites require insulating materials. Therefore, it is necessary to work with filler ratio below p_c.

In previous works, we investigated the influence of electronic irradiations, carried out in space-representative conditions, to the physico-chemical structure of PEEK [17, 18]. We showed that electronic irradiations at room temperature induce cross-linking of the amorphous phase and amorphisation of the crystalline phase. We observed that irradiations in the vicinity of glass transition temperature (165 °C) promotes cross-linking phenomena due to a faster recombination rate of radicals in rubbery state, but does not modify crystalline phase ageing. This allowed us to highlight the significant influence of competition between amorphisation and cross-linking on property evolutions. In this work, we aim to develop PEEK-based composites reinforced with Short Carbon Fibres (SCF) in order to limit surface charging phenomena and to study their behaviour under electronic irradiations, a particular attention will be paid to the evolution of their mechanical and electrical properties. Moreover, these evolutions will be compared to those of the bulk matrix to study the influence of the fibres.

2. Materials and methods

2.1. Materials

For this study, PEEK films (Aptiv 1000 grade) were used in the form of semi-crystalline sheets having a thickness of 100 µm. PEEK/SCF composites were elaborated from the mixing of PEEK pellets (150G grade)

and PEEK/SCF 30 mass % pellets (450CA30 grade). All materials (PEEK films and pellet batches) were supplied by Victrex.

The mixing of pellets was made with a laboratory twin-screw extruder (Haake Minilab II from Thermo Scientific) at a temperature of 360 °C (*i.e.* 20 °C above melting temperature) and with a screw speed of 30 rpm. This speed value was chosen because it enables the mixture to be optimised while maintaining the integrity of the fibres (*i.e.* without damaging their aspect ratio) [19]. The mixing process consists to do a first pass in the extruder of the pellet blend at the desired SCF volumic ratio to obtain pre-mixed extrusion rods. Thereafter, these rods are extruded again in order to homogenise the fibre dispersion. **Figure 1-a** and **Figure 1-b** show SEM images of cryocuts of the resulting extrusion rods, with a SCF ratio of 5 vol. % and 10 vol. % respectively.

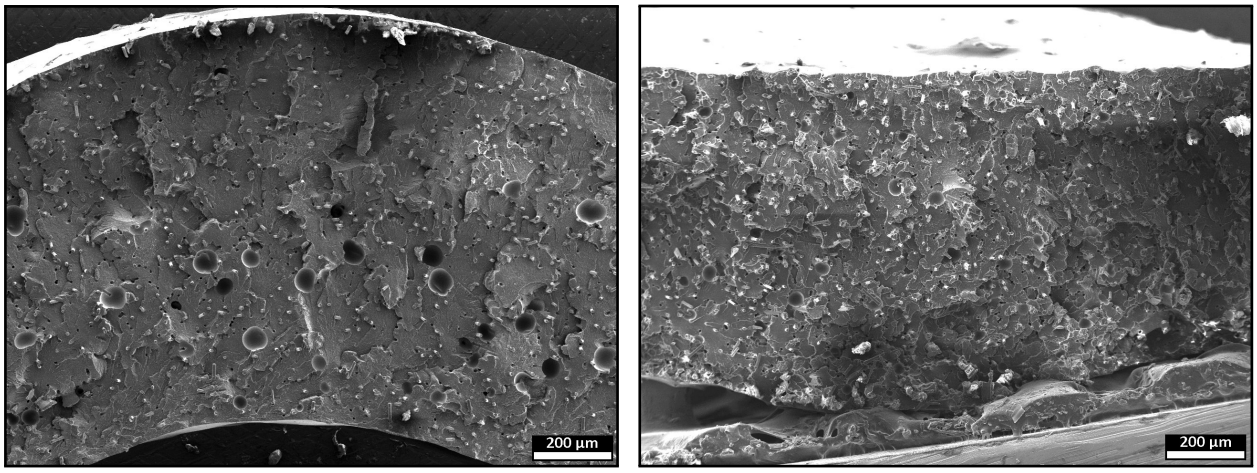

(a) **(b)**

Figure 1: SEM images of extrusion rods with a SCF ratio of 5 vol. % **(a)** and 10 vol. % **(b)**.

These images do not show any fibre bundles or aggregates, this confirms that the mixing protocol used leads to a homogenous fibre dispersion in composites. Moreover, they show that extrusion leads to a preferential orientation of fibres in the polymer melt flow direction. The analyse of multiple SEM images allowed us to measure an average fibre length of (57 ± 8) µm and an average fibre diameter of (7.2 ± 0.5) µm. The resulting aspect ratio is 7.9. Some empty areas (dark areas on images) are also observed and correspond to bubbles introduced in composites during extrusion process.

To determine the percolation threshold p_c, composite samples was elaborated by hot pressing (360 °C, 20 min), in the form of cylinders with a diameter of 20 mm and a thickness between 1 mm and

2 mm, for several fibre ratios in the range [0 ; 16] vol. %. The real part of the dynamic conductivity $\sigma'(\omega)$ was measured by Broadband Dielectric Spectroscopy at 10^{-2} Hz and 25 °C for the different fibre ratios. In this way, p_c was determined at fibre ratio of 9 vol. %. Percolation threshold is proportional to filler aspect ratio ξ according to equation 1 [20, 21].

$$p_c = \frac{0.7}{\xi} \tag{1}$$

The aspect ratio of fibres calculated from this equation is about 7.8. This value is consistent with aspect ratio obtained from SEM image analysis.

However, as explained in introduction, PEEK space applications require electrical insulating materials. Therefore, studied PEEK/SCF composites have to be insulating: *i.e.* the fibre ratio need to be lower than p_c. Thus, the ratio of 3 vol. % was selected to be studied in this work. At this fibre ratio, composite conductivity is about 10^{-13} S.m^{-1} at 10^{-2} Hz. Afterwards, to ensure that the ionising dose deposition is homogenous in our samples, PEEK/SCF 3 vol. % composites were elaborated in the form of 200 µm thick films.

2.2. Experimental irradiations

Samples (PEEK films and composites) were irradiated under high vacuum by a 350 keV mono-energetic electron beam, thanks to SIRENE facility (ONERA, Toulouse, France). PEEK films were irradiated at two temperatures: room temperature and 165 °C, in continuity of our previous work, by using a heating sample-holder (its design has been already described in [18]). Composites were irradiated only at room temperature to study how the fibres influence the ageing of PEEK. The use of high beam current densities (up to 60 nA.cm^{-2}) allowed us to achieve high ionising doses in less than 60 h. The resulting doses D (Gy) were calculated using equation 2 (the detailed stopping power and dose calculations have been already explained in [17]). All doses mentioned afterwards correspond to mean dose in sample thickness.

$$\mathrm{D}\left(\mathrm{Gy} = \mathrm{J.kg^{-1}}\right) = 1.6 \times 10^{-9} \times \Phi \frac{1}{\rho}\left(\frac{d\mathrm{E}}{dx}\right) \tag{2}$$

With Φ the total electronic fluence (electron/cm^2), ρ the material density (g.cm^{-3}) and $d\mathrm{E}/dx$ the electronic stopping power of the material (keV.µm^{-1}).

Two irradiation campaigns were carried out for each type of samples (*i.e.* PEEK films and composites). They lead to ionising doses of 1.2×10^7 MGy and 3.4×10^7 MGy. In these irradiation conditions, the ratios between back and front face doses are 1.5 and 2.1 for PEEK and composite respectively. The dose heterogeneity is higher in composites due to thicker samples (200 µm). However, this degree of heterogeneity is sufficiently low to consider a homogeneous dose deposition in composite thickness.

2.3. Differential Scanning Calorimetry

Differential Scanning Calorimetry (DSC) analyses were carried out on a DSC7 manufactured by PerkinElmer. Analyses were performed under nitrogen flow and consist of two heating runs and one cooling run between 50 °C and 400 °C at a rate of 10 °C.min^{-1}. First-order transition temperatures (melting temperature T_m and crystallisation temperature T_c) were measured at the maximum of the peaks while the glass transition temperature T_g was measured by the tangent method as well as the heat capacity jump ΔC_p. Crystallinity ratio χ_c were determined using equation 3.

$$\chi_c = \frac{\Delta H_m}{\Delta H_\infty (1 - x_f)} \times 100 \tag{3}$$

With ΔH_m the melting enthalpy (J.g^{-1}), ΔH_∞ the theoretical melting enthalpy of a fully crystalline sample reported for PEEK at 130 J.g^{-1} [22] and x_f the weight fraction of fibres which is about 0.04 in PEEK/SCF 3 vol. %.

2.4. Dynamic Mechanical Analysis

Dynamic Mechanical Analyses (DMA) were performed on an ARES G2 strain-controlled rheometer manufactured by TA Instruments. Sample dimensions are 35 mm × 10.5 mm. Due to their low thickness, samples were analysed in tensile geometry mode to ensure a good signal-to-noise ratio. Tests were carried out over the temperature range [–130 ; 250] °C at a rate of 3 °C.min^{-1}. Strain and frequency were fixed at 0.02 % and 1 Hz respectively. In these conditions, samples are solicited in their linearity range allowing us to determine storage $E'_\omega(T)$ and loss $E''_\omega(T)$ moduli.

2.5. Broadband Dielectric Spectroscopy

Broadband Dielectric Spectroscopy (BDS) has been use to analyse electrical behaviour of polymers materials and has already been extensively described [23].

In this work, a Novocontrol BDS 4000 spectrometer associated with an Alpha-A impedance analyser was used to determine DC conductivity and storage permittivity of samples. Samples were prepared in the form of 30 mm diameter film. Analysis were performed over a frequency range of $[10^{-2}\ ;\ 10^{6}]$ Hz and for isotherms going from –150 °C to 250 °C by 5 °C steps. The complex impedance $Z^*(\omega)$ is used to determine the values of sample complex conductivity $\sigma^*(\omega)$ and complex permittivity $\varepsilon^*(\omega)$ using equation 4 and equation 5 respectively.

$$\sigma^* = \sigma' + i\sigma'' = \frac{e}{AZ^*} \tag{4}$$

With e the sample thickness (m) and A its area (m^2).

$$\varepsilon^* = \varepsilon' - i\varepsilon'' = \frac{1}{i\omega C_0 Z^*} \tag{5}$$

With $C_0 = \frac{\varepsilon_0 A}{e}$ where ε_0 is the vacuum permittivity.

By studying the real part of the conductivity $\sigma'(\omega)$, it is possible to determine a DC conductivity σ_{DC} value versus temperature. According to the universal dielectric response formulated by Jonscher [24], the frequency dependence of $\sigma'(\omega)$ in a disordered solid can be describe at a given temperature by equation 6.

$$\sigma'(\omega) = \sigma_{DC} + A.\omega^s \tag{6}$$

At low frequency, the term $A.\omega^s$ becomes negligible in front of σ_{DC} resulting in a frequency-independent conductivity. This phenomena is characterised on $\sigma'(\omega)$ isotherms by the presence of a plateau at low frequency whose value is equal to σ_{DC}. Thus, the σ_{DC} values reported in this work were extracted from these plateaux at a frequency of 10^{-2} Hz. For pristine PEEK and PEEK/SCF 3 vol. %, plateaux are observed above 205 °C and 195 °C respectively. Therefore, charge transport in samples can only be studied above the glass transition temperature by BDS.

2.6. Thermally Stimulated Surface Potential Decay

Thermally Stimulated Surface Potential Decay (TSSPD) is an original approach for studying charge transport in polymer materials. It consists of electrically charging the surface of a sample and following

the decay of the resulting potential during a heating cycle. Initially, samples were charged with positive or negative potentials by using corona processes [25, 26]. Recently, in order to better represent the space environment, Roggero *et al.* used low-energy electrons to build surface charge under high vacuum [27]. This charging process was initially used for Isothermal Potential Decay tests [28].

Experimentally, the PHEDRE facility (ONERA, Toulouse, France) was used. Samples (40 mm) side square) were placed on a copper heating sample-holder under high vacuum (10^{-7} mbar). To ensure a good thermal transfer between samples and their support, a thermally and electrically conductive grease was used. Samples were then charged at room temperature by 20 keV electron beam using a Kimball Physics EMG-4212 electron gun. In these conditions, the average electron implantation depth is about 4 µm. Once charged at ≈–4 kV, a vibrating kelvin probe was used to measure the evolution of sample surface potential U(T) during a heating run at a rate of 4 °C.min^{-1}. The measurement principle of this vibrating kelvin probe is explained in an application note provided by the manufacturer [29]. In the rest of this work, only normalised potential $U(T)/U_0$ will be presented in order to allow the comparison between different assays.

From the evolution of U(T), it is possible to calculate the current density resulting from potential relaxation. Indeed, the current I(t) during relaxation can be calculated in a dielectric material using equation 7.

$$I(t) = C\frac{dU}{dt} \tag{7}$$

Where $C = \varepsilon_0\varepsilon'\frac{A}{e}$ is the sample capacity and $\frac{dU}{dt}$ the time-derivative of surface potential. The current density J(T) (A.m^{-2}) can be calculated using equation 8.

$$J(T) = \frac{\varepsilon_0\varepsilon'_{10^{-2}\,Hz}}{e}\frac{dT}{dt}\frac{dU}{dT} = \frac{\varepsilon_0\varepsilon'_{10^{-2}\,Hz}}{e}\beta\frac{dU}{dT} \tag{8}$$

With $\varepsilon'_{10^{-2}\,Hz}$ the real part of the permittivity obtained by BDS at a frequency of 10^{-2} Hz and β the heating rate (°C.s^{-1}).

3. Results and discussion

3.1. Mechanical behaviour and charge transport in non-irradiated samples

Influence of fibres on mechanical behaviour

Figure 2-a presents the DMA thermograms of pristine PEEK and PEEK/SCF 3 vol. %. For both samples, loss moduli thermograms show two relaxation phenomena. At ≈–90 °C, the relaxation labelled γ is associated with localised mobility and corresponds to dipolar entities on the main chain (*i.e.* ketone groups) which interact with absorbed water [30, 31]. At 150 °C, the intense relaxation labelled α corresponds to the viscoelastic relaxation, *i.e.* the mechanical manifestation of the glass transition. This relaxation is also characterised by a significant drop of the storage modulus.

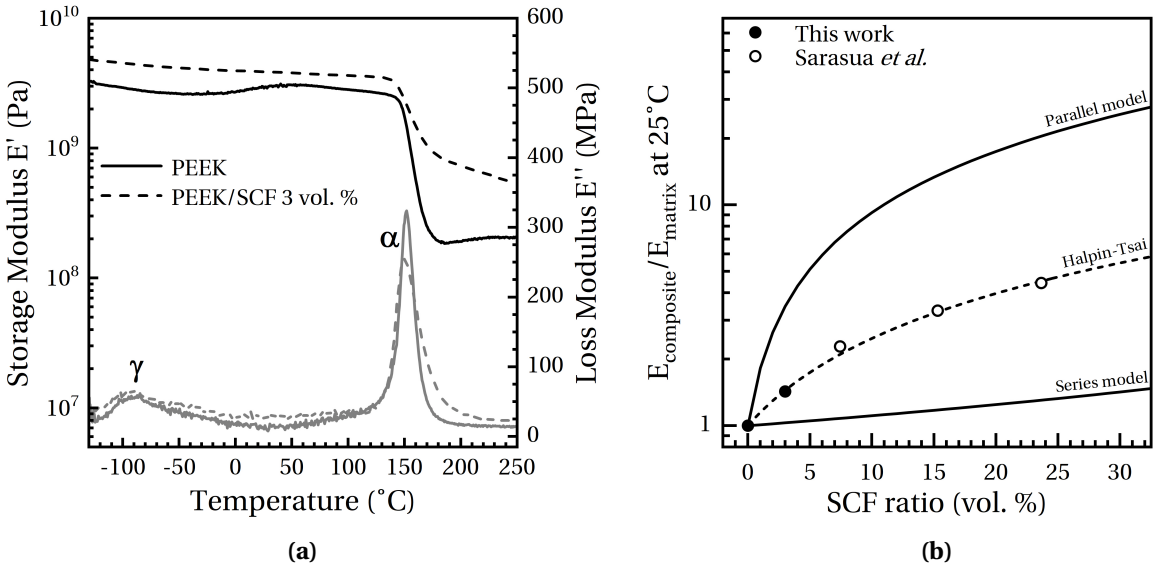

Figure 2: Storage (black) and loss (grey) moduli thermograms of pristine PEEK and pristine PEEK/SCF 3 vol. % **(a)**. Evolution of $E_{composite}/E_{matrix}$ at 25 °C as a function of SCF ratio (empty symbol data were extracted from [32]) compared to different mixing laws **(b)**.

At low temperature, the presence of fibres does not modify the γ relaxation. At higher temperature, α relaxation manifestation temperature is not modified in composite. However, a broadening of the peak is observed as well as an amplitude decrease. The peak area, which is proportional to energy dissipated during the relaxation, is not modified. Thus, this peak broadening is associated with an increase of relaxation time distribution due to fibres which increase heterogeneity around relaxing entities.

An increase in storage modulus in composite is observed over the whole studied temperature range due to the higher modulus of fibres. This increase is about 40 % in glassy state (25 °C) and about 200 % in rubbery state (220 °C). This higher increase in rubbery state has been already observed in polymer composites reinforced by particles with an aspect ratio > 1: fibres play the role of new topological nodes for macromolecules [33, 34].

The evolution of storage modulus in glassy state (25 °C) was studied as a function of SCF ratio. In this work, we experimentally investigate the mechanical behaviour of PEEK (0 vol. % of SCF) and PEEK/SCF 3 vol. %. For higher fibre ratios, data obtained by Sarasua *et al.* was used [32]. In this reference, PEEK/SCF composites were also obtained by extrusion of PEEK/SCF 30 mass % pellets (450CA30) with pure PEEK pellets.

Figure 2-b presents the evolution of $E_{composite}/E_{matrix}$ as a function of fibre ratio. These data were compared to different mixing laws: parallel, series and Halpin-Tsai models.

Parallel and series models consider continuous fibres with an uni-directional orientation. For the parallel model, the mechanical stress is applied along fibre direction. For the series model, the mechanical stress is applied orthogonally to fibre direction. They are described by equation 9 and equation 10 respectively.

$$E_c = E_m(1-\Phi_f) + E_f\Phi_f \tag{9}$$

$$E_c = \left(\frac{1-\Phi_f}{E_m} + \frac{\Phi_f}{E_f}\right)^{-1} \tag{10}$$

With E_c the composite modulus, E_m the matrix modulus, E_f the fibre modulus and Φ_f the volumic ratio of fibres.

The third mixing law used is the Halpin-Tsai model [35, 36] which is described by equation 11. In this model, the parameter θ allows to take into account the influence of filler aspect ratio on the evolution of mechanical modulus. In case of a mechanical stress applied along fibre along fibre direction, $\theta = 2\xi$.

$$E_c = E_m\frac{1+\theta\nu\Phi_f}{1-\nu\Phi_f} \tag{11}$$

With $\nu = \frac{E_f/E_m-1}{E_f/E_m+\theta}$

These three mixing laws are represented in **Figure 2-b** by considering E_m = 2.8 GPa, E_f = 225 GPa [37] et $\theta = 2\xi = 15.8$.

The figure shows that parallel and series models do not describe experimental data at all. This is explained by the hypothesis of the models which consider uni-directionally oriented continuous fibres. Thus, in these conditions, parallel model overestimates modulus values while series model underestimates them. Nonetheless, Halpin-Tsai model gives a good description of data by considering a fibre aspect ratio of 7.9 as calculated from the percolation threshold. This model assumes that stress is applied along fibre direction. Therefore, the fact that it well describes the evolution of glassy modulus with filler ratio indicates that there is a preferential orientation of fibres due to processing.

Influence of fibres on charge transport

The influence of Short Carbon Fibres on the charge transport in pristine samples was studied by ThermallyStimulated Surface Potential Decay below glass transition and by Broadband Dielectric Spectroscopy above glass transition.

Figure 3 presents normalised potential thermograms and the corresponding Current Density obtained by TSSPD for pristine PEEK and PEEK/SCF 3 vol. %.

The PEEK thermogram shows a potential decay which occurs in two steps associated with two relaxation phenomena. The first step is observed on the temperature range [60 ; 140] °C and corresponds to a slow potential decrease. It results in a slight increase of current density up to a plateau from 130 °C. This relaxation phenomenon is associated with the transport of surface electrons through the sample thickness. Indeed, the decrease in the number of electrons implanted at the surface leads to a decrease in measured potential. The second step occurs after 140 °C and is characterised by a sharp decrease in potential, associated with a current density peak centred on 160 °C. In the literature, a similar phenomenon has been observed for a silicone elastomer [27]. It corresponds to a dipolar manifestation of the glass transition. Above glass transition temperature, the increase in macromolecule freedom degrees allows a dipole orientation in the direction of electric field created by surface electrons. This orientation induces an opposed electric field which decreases the apparent electric field. In case of PEEK, the proximity between this phenomenon and the glass transition temperature ($T_g^{ACD} \approx 150$ °C) confirms this explanation.

In PEEK/SCF 3 vol. % composite, the presence of fibres induces significant changes of TSSPD thermogram compared to PEEK. On all the studied temperature range, the normalised potential is lower for composite

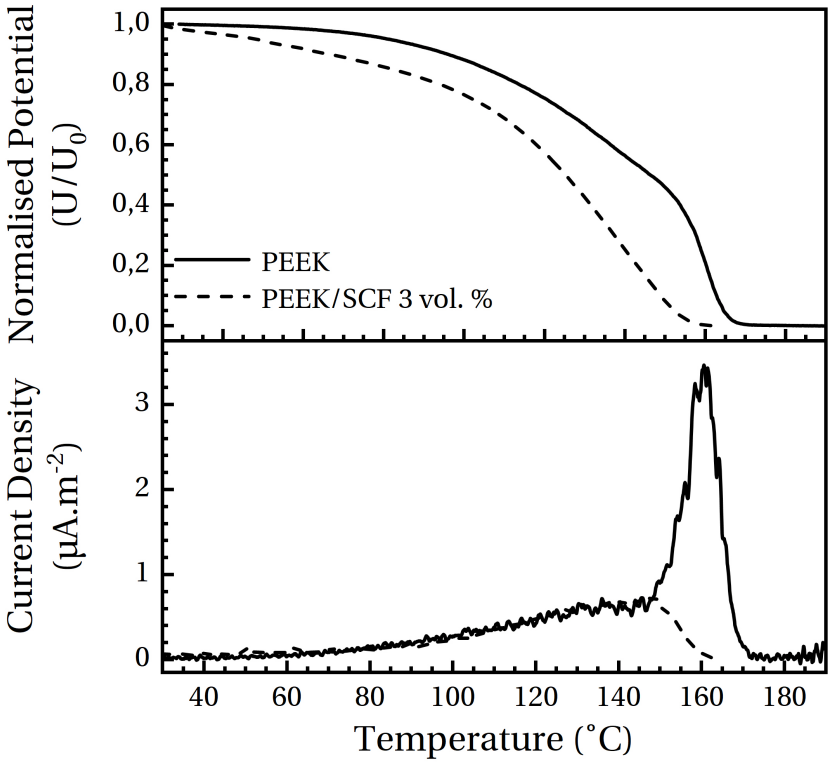

Figure 3: Normalised potential thermograms and corresponding current densities for pristine PEEK and PEEK/SCF 3 vol. %.

than for PEEK. Thus, it appears that the first relaxation phenomenon leads to a faster potential decay, resulting in its total relaxation. This relaxation phenomenon being associated with charge transport in sample thickness, we can conclude that the presence of fibres increases electron conductivity in the composite even below percolation threshold. Moreover, the potential being totally relaxed before the glass transition manifestation, this second phenomenon is not observed. By looking at the current thermogram for composite, the absence of current peak around 160 °C confirms this observation. The figure also shows that during the first relaxation phenomenon, the current density is the same between PEEK and composite despite a faster relaxation process. This is explained by the fact that current density is also proportional to the electric field E ($J = \sigma_{DC}E$). Indeed, despite a higher conductivity thanks to fibres, the electric field is lower: composites are charged with the same initial surface potential as PEEK samples ($U_0 \approx -4$ kV) while their thickness is twice greater.

Figure 4 presents the Arrhenius diagram of σ_{DC} measured by BDS for pristine PEEK and PEEK/SCF 3 vol. %.

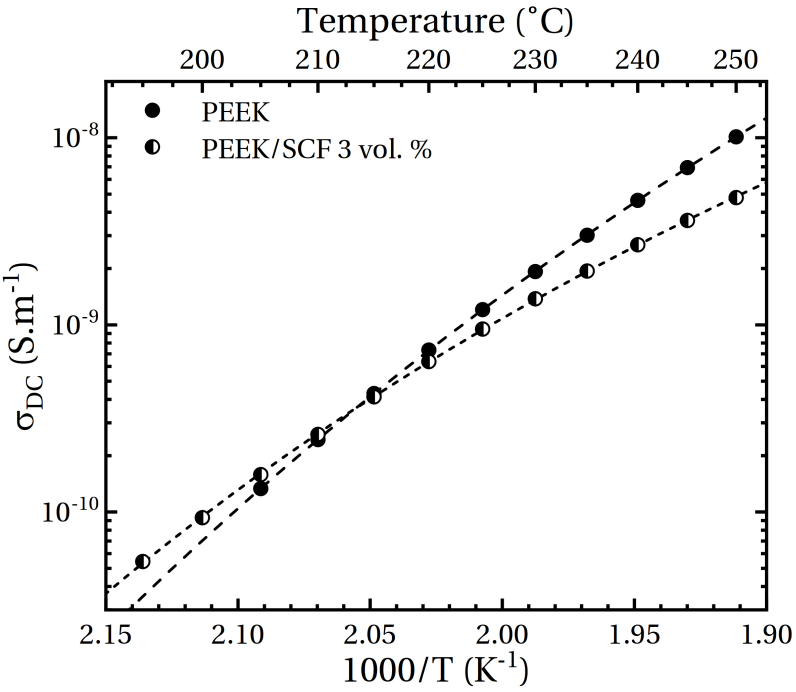

Figure 4: Arrhenius diagram of DC conductivity above glass transition for pristine PEEK and PEEK/SCF 3 vol. %. VTF fit for each samples are represented in dashed lines.

In the literature, Das Gupta and Doughty where the first to study the charge transport in PEEK as a function of temperature [38]. They reported above glass transition temperature an activation energy of 2.1 eV (1 eV = 96 485 J.mol^{-1}). This value is significant in regard to the activation energy measured for several other polymers (*e.g.* ≈0.6 eV for PET [39], ≈0.9 eV for PVDF [40] or ≈0.4 eV for PDMS [27]). They explained this value by the phenyl rings present on the backbone chain of PEEK which limit electron mobility. Afterwards, Kim and Ohki associated this high value with ionic charge carriers predominant above glass transition: ions being larger entities than electrons, the activation energy associated with their conductivity is higher [41]. Similar activation energy value has been already reported and associated with ionic charge carriers: for example Henri *et al.* reported an activation energy of 2.2 eV for a PolyImide [42].

However, for ionic conductive polymers, some studies reported that conductivity can be described by a Vogel-Tammann-Fulcher (VTF) equation above glass transition temperature [43, 44]. This type of temperature behaviour indicates that ionic conductivity is activated by the free volume expansion in the polymer. This VTF behaviour is described by equation 12.

$$\sigma_{DC} = \sigma_{\infty} \exp\left(-\frac{1}{\alpha_f (T - T_0)}\right) \tag{12}$$

With σ_∞ the pre-exponential factor ($S.m^{-1}$), α_f a parameter related to free volume expansion coefficient ($°C^{-1}$) and T_0 the activation temperature of ionic conductivity (°C).

In this work, the VTF fit showed a better description of PEEK σ_{DC} data than an Arrhenius fit on this temperature range. Therefore, we can conclude that the predominant charge carriers in PEEK above glass transition are ions whose transport is activated by the free volume expansion. It should be noted that the α mobility in PEEK, corresponding to the glass transition manifestation, follows a VTF behaviour as well [18, 45]. Thus, in PEEK, α mobility and ionic conductivity above T_g are both activated by the same process: the free volume expansion. In regards of PEEK chemical structure, it can be assumed that ions correspond to protons released from the aromatic rings due to temperature increase; the resulting negative charge is stabilised by electron delocalisation. For composites, the same temperature dependence of conductivity is observed. This indicates that the main charge carriers above glass transition remain ions even in presence of carbon fibres. Thus, fit parameters obtained for pristine PEEK and PEEK/SCF 3 vol. % are reported in Table 2.

For PEEK, the α_f value is consistent with the one found in a previous study through the VTF fit of α relaxation ($\alpha_f = 4.4 \times 10^{-4}$ °C^{-1}) [18]. A similar value is also found for composite. This confirms that the ion transport is activated by the same macromolecular process, *i.e.* the free volume expansion. However, a lower activation temperature is found for ionic conductivity than for α relaxation (T_∞ = 90 °C), either in PEEK or PEEK/SCF 3 vol. %. In the literature, similar activation temperatures for this two process have been observed for a PolyEpoxy [43] and for a PolyThioPhene / PolyVinylAcetate composite [44].In the free volume theory, this temperature is described as the temperature at which the free volume became higher than a critical volume above which the process is possible [46]. For both of the listed systems, the critical volume allowing the α relaxation process is the same than for the activation of ionic transport. However, the α relaxation of PEEK occurs at high temperatures due to the rigidity of the main chain. The ion size being small compared to α relaxing entities, the free critical volume associated with their transport is reached at lower temperatures: $T_0 < T_\infty$.

Between PEEK and PEEK/SCF 3 vol. %, the σ_{DC} values are very close. This is explain by the fact that carbon fibres are not ionic conductors and therefore, do not modify the ion conductivity. However, the fibre have an influence on the VTF fit parameters T_0 and α_f. An increase in T_0 is observed in composite and indicates that in presence of fibres, the activation of conductivity by the free volume occurs at higher

temperature. Nonetheless, once the activation temperature is reached, the free volume expansion is higher (*i.e.* increase in α_f).

3.2. Influence of fibres on ageing mechanisms of PEEK under electronic irradiations

In previous studies, we showed by calorimetric analyses that amorphisation of crystallites and cross-linking of amorphous phase occur in PEEK when irradiated by electrons [17, 18]. The amorphisation process was highlighted by the decrease in melting temperature T_m and in crystallinity ratio χ_c. The cross-linking was identified by the increase in glass transition temperature T_g and by the irreversibility of modifications (*e.g.* the decrease in T_m observed on first and second heating scan).

DSC analyses were also carried out on PEEK/SCF 3 vol. % composites in order to identify the influence of fibres on the ageing of PEEK matrix. However, DSC thermograms are not presented here for the sake of clarity. Instead, data extracted from these thermograms are reported in Table 1 and their evolutions with dose in PEEK and PEEK/SCF 3 vol. % are compared in **Figure 5**.

Table 1: Data extracted from DSC analyses of pristine, irradiated PEEK and PEEK/SCF 3 vol. %. 1^{st} refers to first heating runs and 2^{nd} to second heating runs.

	T_g (°C)		ΔC_p ($J.g^{-1}.°C^{-1}$)		T_m (°C)		χ_c (%)		T_c (°C)
	1^{st}	2^{nd}	1^{st}	2^{nd}	1^{st}	2^{nd}	1^{st}	2^{nd}	
PEEK									
Pristine	158	147	0.15	0.14	339	339	34.1	40.1	297
Dose 12 MGy	157	150	0.11	0.12	331	333	32.6	33.7	286
Dose 34 MGy	159	153	0.16	0.16	318	320	25.8	23.0	269
PEEK/SCF 3 vol. %									
Pristine	151	147	0.13	0.11	341	342	35.8	40.1	299
Dose 12 MGy	154	150	0.08	0.11	332	333	34.5	35.2	282
Dose 34 MGy	159	153	0.10	0.13	323	320	30.9	29.7	265

In presence of fibres, the evolutions of these thermal parameters follow the same trend than PEEK like described before. Thus, for this SCF ratio, fibres do not modify the ageing mechanisms of PEEK.

Specifically, **Figure 5** shows that the increase in T_g during the second heating run is the same than for PEEK: the evolution of cross-linking density with dose is not modified. The decrease in crystallisation temperature T_c (shown in Table 1) is similar to the one observed in PEEK. This decrease is linked to the

increase in cross-linking and therefore is consistent with the increase in T_g. In the crystalline phase, a significant difference in crystallinity ratio is noticed between pristine samples: a higher χ_c is observed for the composite and explained by fibres which play the role of nucleation sites leading to a higher quantity of crystalline phase. After irradiations, a slightly lower decrease in T_m is observed, especially fo the highest dose. Fibres seem to stabilise the crystallite ageing. This hypothesis is confirmed by the lower decrease in the crystallinity ratio of composite in front of PEEK samples. During the second heating run, T_m is the same for PEEK and PEEK/SCF 3 vol. %: cross-linking of amorphous phase limits the crystallite growth. However, the crystallinity ratio remains higher in irradiated composites. This is due to the fibres which still act as nucleation sites during cooling from melting state.

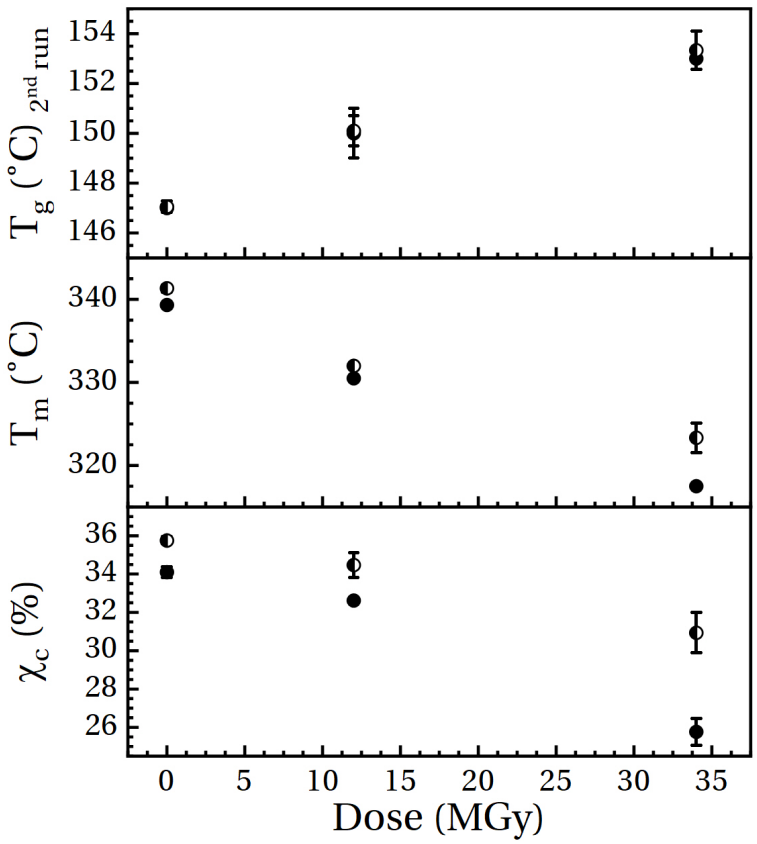

Figure 5: Thermal parameters extracted from DSC thermograms as a function of dose for PEEK (full symbols) and PEEK/SCF 3 vol. % (half-empty symbols).

The influence of this physico-chemical ageing on the mechanical behaviour of composites was studied by DMA. Storage E' and loss E" moduli thermograms are presented in **Figure 6** for pristine and irradiated PEEK/SCF 3 vol. %.

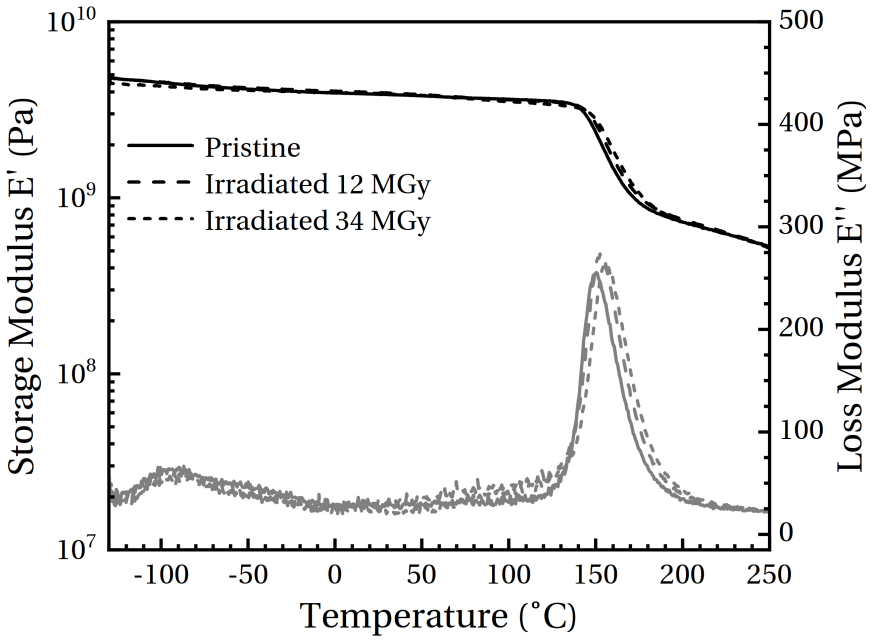

Figure 6: Storage (black) and loss (grey) moduli thermograms of pristine and irradiated PEEK/SCF 3 vol. %.

On the loss modulus thermograms, the γ relaxation is not modified by ageing. This behaviour was also observed for PEEK samples and was linked to the fact that distance between cross-linking nodes is larger than the size of involved relaxing entities. On the α relaxation, irradiations induce a shift of the peak to higher temperatures. This increase is similar in PEEK and is consistent with the increase in T_g. It is explained by the cross-links which limit the mobility of chain sequences relaxing at T_α.

On the storage modulus thermograms, the presence of fibres has a significant influence on their evolution after irradiations. Contrary to PEEK for which a significant increase in rubber modulus due to cross-linking phenomenon was reported, no evolution either glassy modulus or rubber modulus is observed in irradiated composites. Thus, the presence of fibres stabilises the evolution of composite mechanical behaviour. This absence of evolution can be explained by two contributions. In one hand, fibres stabilise the ageing of the matrix under electronic irradiations and therefore, stabilise the evolution of mechanical behaviour. On the other hand, the presence of fibres hides the influence of matrix ageing on mechanical behaviour of the composite.

3.3. Evolution of charge transport in irradiated PEEK and PEEK / Short Carbon Fibre composite

The influence of electronic irradiations on charge transport in PEEK and PEEK/SCF 3 vol. % composite was studied below and above glass transition temperature. In case of PEEK, the influence of irradiations in rubbery state ($T_{irrad.}$ = 165 °C) was also investigated in the continuity of our previous work.

Charge transport below glass transition

Figure 7 present the normalised potential thermograms for both materials and for each irradiations conditions.

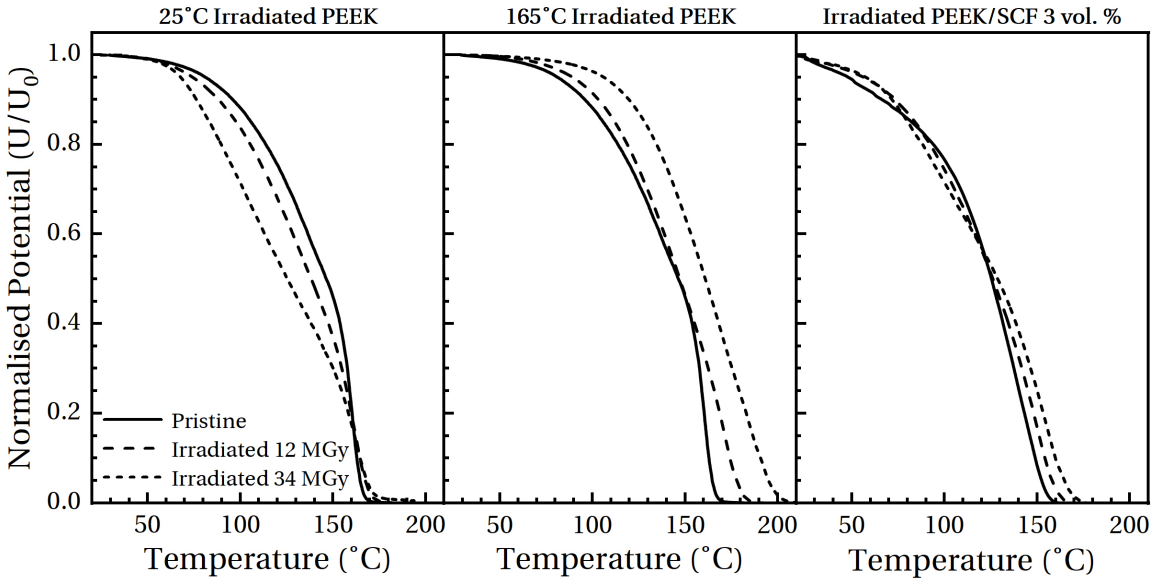

Figure 7: Normalised potential thermograms for 25 °C irradiated PEEK (left), 165 °C irradiated PEEK (center) and irradiated PEEK/SCF 3 vol. % (right).

For PEEK samples, room temperature irradiations induce a shift to lower temperatures of the first relaxation phenomena with increasing dose. It means that electronic transport occurs earlier after ageing. In PolyPropylene, Thyssen showed that the decrease in crystallinity ratio leads to an earlier surface potential relaxation [47]: conductivity in polymers taking place in amorphous phase, the increase in amorphous quantity favours charge transport. In addition, this shift to lower temperature can also be partly explained by a decrease in the activation energy of this relaxation phenomenon. A decrease in the slope of the potential decay is observed as well (*i.e.* a decrease in the corresponding current density). Ageing induces a decrease in electronic conductivity which is explained by the increase in the quantity of

charge traps. On the dipolar manifestation of the glass transition, we can denote a slight increase in the width of the potential drop. This is explained by a more heterogeneous medium around relaxing entities.

After irradiation at 165 °C, a shift of the whole thermogram to higher temperature with increasing dose is observed. This evolution is explained by the increase in charge traps associated with the increase in the number of cross-linking nodes. This behaviour is totally opposite to the one observed after room temperature irradiations. This is due to the higher cross-linking density whose effect becomes predominant in front of amorphisation effect. Similar trends have been observed in PEEK for other properties like penetrant diffusion [18]. These observations confirm that competition between amorphisation and cross-linking has a significant influence on polymer property evolutions under electronic radiations and more generally under ionising radiations.

For PEEK/SCF 3 vol. % composites, irradiated sample thermograms are very similar to the pristine one, regardless of the ionising dose. It shows that the presence of fibres tends to stabilise the surface relaxation process in front of electronic irradiations. This behaviour is analogous to the one observed through mechanical analysis and is explained in the same way by two contributions: a stabilisation of the matrix ageing and the hiding of ageing influence on electronic transport. This last part illustrates the fact that fibres tend to control the electronic conductivity, even below the percolation threshold.

Charge transport above glass transition

Figure 8 presents the Arrhenius diagrams of σ_{DC} above T_g for pristine / irradiated PEEK (**Figure 8-a**), and for pristine / irradiated PEEK/SCF 3 vol. % (**Figure 8-b**). VTF fit are represented in dashed lines and fit parameters are reported in Table 2 for both PEEK and PEEK/SCF 3 vol. % composites.

For PEEK samples, room temperature irradiations lead to a decrease in σ_{DC} with increasing dose on all the temperature range. A simultaneous decrease in $\sigma_{\infty,\nu}$ is observed. For 165 °C irradiated PEEK, a greater decrease is observed: for the highest dose, this decrease is about one decade. These evolutions coincide with the increase in cross-linking density in PEEK: a higher cross-linking density induces a higher decrease in ionic conductivity. It is explained by cross-linking nodes which limits ionic transport by decreasing amorphous phase mobility.

Moreover, we observe that for 165 °C irradiations, PEEK σ_{DC} temperature behaviour tends to an Arrhenius behaviour. This change is observed as well through the significant decrease in T_0 parameter. Indeed, when T_0 = 0 K the VTF equation becomes a typical Arrhenius equation. However, an opposite evolution

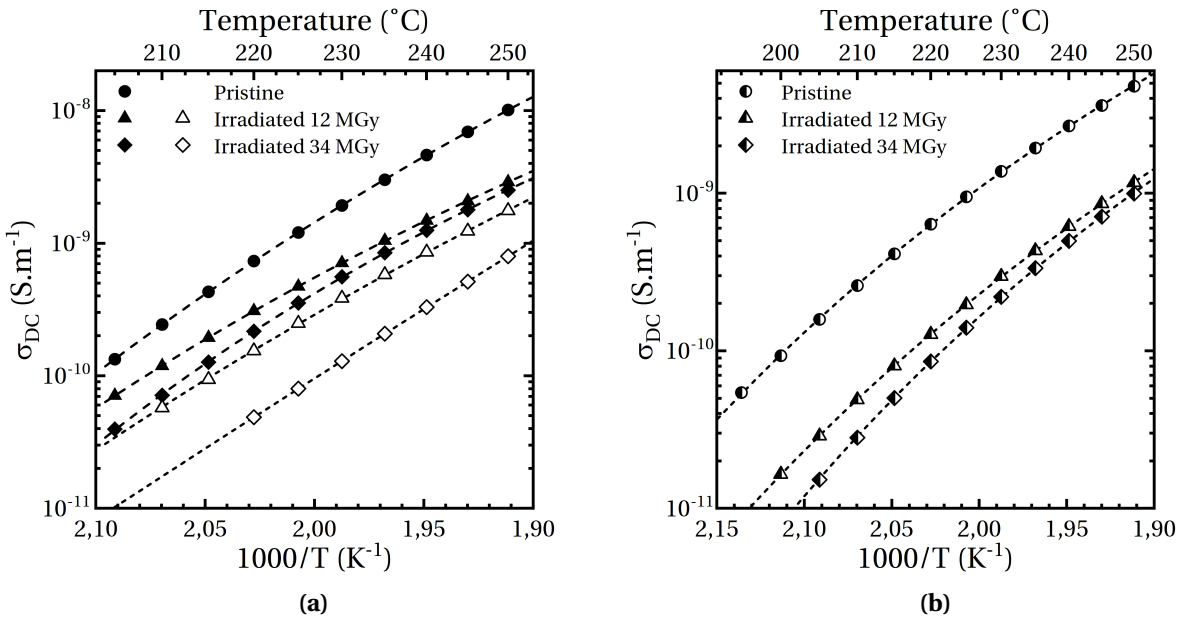

Figure 8: Arrhenius diagram of σ_{DC} for pristine, 25 °C irradiated (full symbols) and 165 °C irradiated (empty symbols) PEEK **(a)**, and for pristine and 25 °C irradiated PEEK/SCF 3 vol. % **(b)**. VTF fit are represented in dashed lines.

is observed after room temperature irradiations with an increase in T_0 with dose. In this case, the T_0 increase is associated with the increase in cross-linking nodes which constrain the free volume and is coherent with the increase in T_g. For 165 °C irradiated samples, the change towards an Arrhenius behaviour indicates that ionic conductivity becomes less and less dependent on molecular mobility. To the author's knowledge, this trend has never been reported in literature. It can be supposed that the higher stiffening of amorphous phase due to higher cross-linking density limits the influence of molecular mobility on ionic transport.

On the α_f parameter, opposite evolutions between both irradiation temperatures are observed as well: an increase for 25 °C irradiations and a decrease for 165 °C irradiations. Again, this behaviour is explained by the competition between amorphisation and cross-linking. For room temperature irradiations, the effect of amorphisation is predominant: the lower quantity of crystallites induces less constrains on amorphous phase and favours free volume expansion (α_f increase). For 165 °C irradiations, the effect of cross-linking becomes predominant and limits the free volume expansion (α_f decrease).

In PEEK/SCF 3 vol. % composites, a decrease in σ_{DC} (along with a decrease in $\sigma_{\infty,v}$) with increasing dose is observed as well. This decrease is slightly higher than in room temperature irradiated PEEK. In contrast to electronic transport, the presence of carbon fibres does not stabilise the evolution of ionic conductivity

under electronic irradiations. This is consistent with the observations made between pristine PEEK and PEEK/SCF 3 vol. % samples: since carbon fibres are not ionic conductors, ion transport stay driven by the matrix properties. Therefore, in pristine state, fibres have no influence on σ_{DC} values while after irradiations, the matrix ageing leads to a decrease in σ_{DC}.

Some evolutions on fit parameters are observed. On the T_0 parameter, a tendency to increase is observed after 34 MGy. As for PEEK, cross-links limit the free volume increase. However, no significant evolution of α_f is observed for irradiated PEEK/SCF 3 vol. % in contrast to PEEK.

Table 2: VTF parameters obtained from the fit of σ_{DC} for pristine, irradiated PEEK and PEEK/SCF 3 vol. %.

	PEEK			**PEEK/SCF 3 vol. %**		
	$\sigma_{\infty,v}$	α_f	T_0	$\sigma_{\infty,v}$	α_f	T_0
	($S.m^{-1}$)	($°C^{-1}$)	(°C)	($S.m^{-1}$)	($°C^{-1}$)	(°C)
Pristine	2.7×10^{-2}	3.45×10^{-4}	51	8.8×10^{-5}	5.75×10^{-4}	75
25 °C Irradiation						
Dose 12 MGy	4.2×10^{-4}	4.54×10^{-4}	61	7.3×10^{-5}	5.07×10^{-4}	71
Dose 34 MGy	9.2×10^{-5}	6.17×10^{-4}	92	5.5×10^{-5}	5.75×10^{-4}	88
165 °C Irradiation						
Dose 12 MGy	1.7×10^{-2}	2.78×10^{-4}	23	∅	∅	∅
Dose 34 MGy	9.9×10^{6}	0.63×10^{-4}	–178	∅	∅	∅

4. Conclusion

The aim of this work was to elaborate PEEK / SCF composites in order to limit surface charging in space environment and to study their ageing under electronic irradiations (compared to the ageing of bulk PEEK). The fibre percolation threshold was determined at 9 vol. %. PEEK space applications requiring insulator materials, the SCF ratio selected for this study is 3 vol. %.

In pristine state, fibres induce an increase in glassy and rubbery moduli compared to PEEK. This increase is higher in rubbery state because fibres play the role of additional entanglements. The influence of fibres on charge transport was studied above and below glass transition temperature. Below T_g, the presence of fibres induces a faster potential relaxation compared to PEEK. Fibres favour electronic transport, even below percolation threshold. This behaviour shows that SCF can reduce ESD risks by decreasing electron accumulation. Above T_g, BDS showed that predominant charge carriers are ions whose transport is activated by free volume. In composite, fibres do not modify σ_{DC} values. This is due to the fact that

fibres are not ionic conductors and therefore, dot not participate in ionic transport. However, this is not problematic in regards to charging issue because σ_{DC} values above T_g is high enough to limit electronic accumulation.

After irradiations, calorimetric analysis showed that PEEK ageing mechanisms are not modified by the presence of fibres: amorphisation and cross-linking. The study of composite mechanical behaviour after irradiations showed very slight changes compared to PEEK. Especially, no evolution of storage modulus with dose was observed. This is due to fibres which stabilise the composite mechanical behaviour under irradiation. This stabilisation comes from two contributions: fibres stabilise the ageing of the matrix and hides the influence of this ageing on mechanical behaviour.

Below T_g, irradiation temperature has a significant influence on potential relaxation in PEEK: 25 °C irradiations induce a shift to lower temperature while 165 °C irradiations induce a shift to higher temperature. It is explained by the competition between amorphisation and cross-linking. In composite, like for mechanical behaviour, fibres stabilise the potential relaxation: fibres control electronic transport. Therefore, even after ageing, SCF continue to limit ESD risks. Above T_g, a decrease in σ_{DC} is observed in PEEK (with a higher decrease after 165 °C irradiations) and in composite (ionic transport is controlled by the matrix properties). This decrease is linked to the increase in cross-linking density.

Acknowledgement

The authors would like to thank CNES for technical support (funding of the SIRENE facility) as well as Région Occitanie and ONERA for financial support in this project.

References

[1] A.-M. Lanouette, M.-J. Potvin, F. Martin, D. Houle, D. Therriault, Residual mechanical properties of a carbon fibers/PEEK space robotic arm after simulated orbital debris impact, Int. J. Impact Eng. 84 (2015) 78–87. doi:10.1016/j.ijimpeng.2015.05.010.

[2] S. D. Bale, K. Goetz, P. R. Harvey, P. Turin, J. W. Bonnell, T. Dudok de Wit *et al.*, The FIELDS Instrument Suite for Solar Probe Plus: Measuring the Coronal Plasma and Magnetic Field, Plasma Waves and Turbulence, and Radio Signatures of Solar Transients, Space Sci. Rev. 204 (2016) 49–82. doi:10.1007/s11214-016-0244-5.

[3] E.-S. A. Hegazy, T. Sasuga, M. Nishii, T. Seguchi, Irradiation effects on aromatic polymers: 1. Gas evolution by gamma irradiation, Polymer 33 (1992) 2897–2903. doi:10.1016/0032-3861(92)90074-7.

[4] E.-S. A. Hegazy, T. Sasuga, M. Nishii, T. Seguchi, Irradiation effects on aromatic polymers: 2. Gas evolution during electron-beam irradiation, Polymer 33 (1992) 2904–2910. doi:10.1016/0032-3861(92)90075-8.

[5] E.-S. A. Hegazy, T. Sasuga, T. Seguchi, Irradiation effects on aromatic polymers: 3. Changes in thermal properties by gamma irradiation, Polymer 33 (1992) 2911–2914. doi:10.1016/0032-3861(92)90076-9.

[6] T. Sasuga, N. Hayakawa, K. Yoshida, M. Hagiwara, Degradation in tensile properties of aromatic polymers by electron beam irradiation, Polymer 26 (1985) 1039–1045. doi:10.1016/0032-3861(85)90226-5.

[7] T. Sasuga, M. Hagiwara, Mechanical relaxation of crystalline poly(aryl-ether-ether-ketone) (PEEK) and influence of electron beam irradiation, Polymer 27 (1986) 821–826. doi:10.1016/0032-3861(86)90288-0.

[8] K. Shinyama, M. Baba, S. Fujita, Dielectric properties of electron beam irradiated polymer insulating material, in: Proceedings of 1998 International Symposium on Electrical Insulating Materials. 1998 Asian International Conference on Dielectrics and Electrical Insulation. 30th Symposium on Electrical Insulating Materials, Institute of Electrical Engineers of Japan, Toyohashi, Japan, 1998. doi:10.1109/ISEIM.1998.741765.

[9] K. Shinyama, S. Fujita, Dielectric and thermal properties of irradiated polyetheretherketone, IEEE T. Dielect. El. In. 8 (2001) 538–542. doi:10.1109/94.933380.

[10] R. D. Leach, Failures and Anomalies Attributed to Spacecraft Charging, Tech. Rep. Tech. Rep. NASA-RP-1375, NASA Marshall Space Flight Center (1995).

[11] M. Mokhtari, E. Archer, N. Bloomfield, E. Harkin-Jones, A. McIlhagger, High-performance and cost-effective melt blended poly(ether ether ketone)/expanded graphite composites for mass production of antistatic materials, Polym. Int. doi:10.1002/pi.6226.

[12] S. Khan, L. Lorenzelli, Recent advances of conductive nanocomposites in printed and flexible electronics, Smart Mater. Struct. 26 (2017) 083001. doi:10.1088/1361-665X/aa7373.

[13] T. Wang, Y. Zhang, Q. Liu, W. Cheng, X. Wang, L. Pan *et al.*, A Self-Healable, Highly Stretchable, and Solution Processable Conductive Polymer Composite for Ultrasensitive Strain and Pressure Sensing, Adv. Funct. Mater. 28 (2018) 1705551. doi:10.1002/adfm.201705551.

[14] L. Quiroga Cortés, S. Racagel, A. Lonjon, E. Dantras, C. Lacabanne, Electrically conductive carbon fiber / PEKK / silver nanowires multifunctional composites, Compos. Sci. Technol. 137 (2016) 159–166. doi:10.1016/j.compscitech.2016.10.029.

[15] V. Bedel, A. Lonjon, E. Dantras, M. Bouquet, Innovative conductive polymer composite coating for aircrafts lightning strike protection, J. Appl. Polym. Sci. 137 (2020) 48700. doi:10.1002/app.48700.

[16] S. Kirkpatrick, Percolation and Conduction, Rev. Mod. Phys. 45 (1973) 574–588. doi:10.1103/RevModPhys.45.574.

[17] G. Rival, T. Paulmier, E. Dantras, Influence of electronic irradiations on the chemical and structural properties of PEEK for space applications, Polym. Degrad. Stab. 168 (2019) 108943. doi:10.1016/j.polymdegradstab.2019.108943.

[18] G. Rival, E. Dantras, T. Paulmier, Electronic irradiation ageing in the vicinity of glass transition temperature for PEEK space applications, Polym. Degrad. Stab. 181 (2020) 109305. doi:10.1016/j.polymdegradstab.2020.109305.

[19] D. Carponcin, E. Dantras, G. Aridon, F. Levallois, L. Cadiergues, C. Lacabanne, Evolution of dispersion of carbon nanotubes in Polyamide 11 matrix composites as determined by DC conductivity, Compos. Sci. Technol. 72 (2012) 515–520. doi:10.1016/j.compscitech.2011.12.012.

[20] I. Balberg, N. Binenbaum, N. Wagner, Percolation Thresholds in the Three-Dimensional Sticks System, Phys. Rev. Lett. 52 (1984) 1465–1468. doi:10.1103/PhysRevLett.52.1465.

[21] I. Balberg, S. Alexander, N. Wagner, Excluded volume and its relation to the onset of percolation, Phys. Rev. B 30 (1984) 3933–3943. doi:10.1103/PhysRevB.30.3933.

[22] D. J. Blundell, B. N. Osborn, The morphology of poly(aryl-ether-ether-ketone), Polymer 24 (1983) 953–958. doi:10.1016/0032-3861(83)90144-1.

[23] F. Kremer, A. Schönhals, Broadband Dielectric Spectroscopy, Springer, Berlin, 2003.

[24] A. K. Jonscher, The "universal" dielectric response, Nature 267 (1977) 673–679. doi:10.1038/267673a0.

[25] T. Mizutani, T. Oomura, M. Ieda, Surface Potential Decay in Polyethylene, Jpn. J. Appl. Phys. 20 (1981) 855–859. doi:10.1143/JJAP.20.855.

[26] H. von Berlepsch, M. Pinnow, Thermally stimulated surface potential decay in HDPE and the cross-over phenomenon, Phys. Status Solidi A 105 (1988) 485–492. doi:10.1002/pssa.2211050221.

[27] A. Roggero, E. Dantras, T. Paulmier, C. Tonon, N. Balcon, V. Rejsek-Riba *et al.*, Electrical behaviour of a silicone elastomer under simulated space environment, J. Phys. D Appl. Phys. 48 (2015) 135302. doi:10.1088/0022-3727/48/13/135302.

[28] T. Paulmier, B. Dirassen, M. Belhaj, D. Rodgers, Charging Properties of Space Used Dielectric Materials, IEEE T. Plasma Sci. 43 (2015) 2894–2900. doi:10.1109/TPS.2015.2453012.

[29] M. A. Noras, Non-contact surface charge/voltage measurements. Capacitive probe - principle of operation, Trek Application Note n°3001 (2002) 1–8.

[30] J. E. Harris, L. M. Robeson, Miscible blends of poly(aryl ether ketone)s and polyetherimides, J. Appl. Polym. Sci. 35 (1988) 1877–1891. doi:10.1002/app.1988.070350713.

[31] M. Coulson, L. Quiroga Cortés, E. Dantras, A. Lonjon, C. Lacabanne, Dynamic rheological behavior of poly(ether ketone ketone) from solid state to melt state, J. Appl. Polym. Sci. 135 (2018) 46456. doi:10.1002/app.46456.

[32] J. R. Sarasua, P. M. Remiro, J. Pouyet, The mechanical behaviour of PEEK short fibre composites, J. Mater. Sci. 30 (1995) 3501–3508. doi:10.1007/BF00349901.

[33] F. Dalmas, J.-Y. Cavaillé, C. Gauthier, L. Chazeau, R. Dendievel, Viscoelastic behavior and electrical properties of flexible nanofiber filled polymer nanocomposites. Influence of processing conditions, Compos. Sci. Technol. 67 (2007) 829–839. doi:10.1016/j.compscitech.2006.01.030.

[34] A. Lonjon, P. Demont, E. Dantras, C. Lacabanne, Mechanical improvement of P(VDF-TrFE) /nickel nanowires conductive nanocomposites: Influence of particles aspect ratio, J. of Non-Cryst. Solids 358 (2012) 236–240. doi:10.1016/j.jnoncrysol.2011.09.019.

[35] J. Halpin, J. Kardos, Moduli of Crystalline Polymers Employing Composite Theory, J. Appl. Phys. 43 (1972) 2235–2241. doi:10.1063/1.1661482.

[36] J. Halpin, J. L. Kardos, The Halpin-Tsai equations: A review, Polym. Eng. Sci. 16 (1976) 344–352. doi:10.1002/pen.760160512.

[37] L. N. McCartney, Predicting Properties of Undamaged and Damaged Carbon Fibre Reinforced Composites, in: P. W. R. Beaumont, C. Soutis, A. Hodzic (Eds.), The Structural Integrity of Carbon Fiber Composites, Springer International Publishing, Cham, 2017, pp. 425–467. doi:10.1007/978-3-319-46120-5_16.

[38] D. Das-Gupta, K. Doughty, Dielectric and Conduction Processes in Polyetherether Ketone (PEEK), IEEE T. Electr. Insul. EI-22 (1987) 1–7. doi:10.1109/TEI.1987.298955.

[39] D. Das-Gupta, K. Joyner, On the nature of absorption currents in polyethyleneterephthalate (PET), J. Phys. D Appl. Phys. 9 (1976) 829–840. doi:10.1088/0022-3727/9/5/016.

[40] D. Das-Gupta, K. Doughty, R. S. Brockley, Charging and discharging currents in polyvinylidene fluoride, J. Phys. D Appl. Phys. 13 (1980) 2101–2114. doi:10.1088/0022-3727/13/11/020.

[41] E. Kim, Y. Ohki, Ionic behavior of dc conduction in polyetheretherketone, IEEE T. Dielect. El. In. 2 (1995) 74–83. doi:10.1109/94.368682.

[42] V. Henri, E. Dantras, C. Lacabanne, F. Koliatene, C. Trebosc, Ageing of Polyimide under thermal stress: relaxationnal effects and charge transport, Polymer Degradation and Stability 186 (2021) 109524. doi:10.1016/j.polymdegradstab.2021.109524.

[43] G. A. Kontos, A. L. Soulintzis, P. K. Karahaliou, G. C. Psarras, S. N. Georga, C. A. Krontiras *et al.*, Electrical relaxation dynamics in TiO2 – polymer matrix composites, Express Polym. Lett. 1 (2007) 781–789. doi:10.3144/expresspolymlett.2007.108.

[44] R. Bobade, S. Pakade, S. Yawale, Electrical investigation of polythiophene–poly(vinyl acetate) composite films via VTF and impedance spectroscopy, J. Non-Cryst. Solids 355 (2009) 2410–2414. doi:10.1016/j.jnoncrysol.2009.08.041.

[45] J. Audoit, L. Rivière, J. Dandurand, A. Lonjon, E. Dantras, C. Lacabanne, Thermal, mechanical and dielectric behaviour of poly(aryl ether ketone) with low melting temperature, J. Therm. Anal. Calorim. 135 (2018) 2147–2157. doi:10.1007/s10973-018-7292-x.

[46] M. H. Cohen, D. Turnbull, Molecular Transport in Liquids and Glasses, J. Chem. Phys. 31 (1959) 1164–1169. doi:10.1063/1.1730566.

[47] A. Thyssen, Charge distribution and stability in electret materials, Ph.D. thesis, Denmark Technical University, DTU Nanotech (2016).